

Random nonequilibrium Green's function method for large-scale quantum transport simulation

Qingyun Zhang ¹, Mingfa Tang, ¹ Lei Wang ², Ke Xia, ² and Youqi Ke ^{1,*}

¹School of Physical Science and Technology, ShanghaiTech University, Shanghai, 201210, China

²Department of Physics, Southeast University, Nanjing 100193, China



(Received 4 July 2024; revised 14 September 2024; accepted 1 October 2024; published 21 October 2024)

We report a random nonequilibrium Green's function method (rNEGF) to tackle the challenge of large-scale quantum transport simulation. In this method, the rNEGF is represented with N_s random superposition states of the source eigenmodes, significantly reducing the computational complexity of quantum transport properties. As a demonstration, we implement the rNEGF within the exact muffin-tin orbital-based density functional theory and calculate the electron transmission through large devices with Hamiltonian dimension up to 4×10^5 from first principles. It is found that a rather small N_s (even $N_s = 1$), in orders of magnitude smaller than the number of source eigenmodes, can present reliable transmission results with a relative standard deviation $\sim 1\%$. Our calculations cover the challenging transport regimes of disorder scattering and resonant tunneling. The rNEGF method only bares the statistical error and presents an important self-averaging effect with respect to the cross-section size of the device, providing an effective stochastic quantum transport approach.

DOI: [10.1103/PhysRevB.110.155430](https://doi.org/10.1103/PhysRevB.110.155430)

The nonequilibrium Green's function (NEGF) method provides a comprehensive framework for addressing nonequilibrium quantum statistics and managing complex interactions [1–6]. As a representative application, NEGF provides nonequilibrium density matrix for self-consistent calculation of electronic structures and provides quantum transport properties of electronic devices. As the device shrinks to the nanometer scale, it requires discrete atomistic modeling, and the quantum effects, e.g., confinement, tunneling, and interference, necessitate a fully quantum mechanical treatment [7]. The NEGF method, combined with Kohn-Sham density functional theory (DFT) [8–15] and tight-binding (TB) models [7,16–18], has been developed as the workhorse for quantum transport simulations, and NEGF-DFT/TB methods emerge as the core technology in atomistic TCAD (technology computer-aided design) for the modern semiconductor industry. However, the current computational complexity of NEGF, for a device with a cross-section size of $N_x N_y$ and a length size of N_z , scales as $O[(N_x N_y)^3 N_z]$ with the recursive GF technique [19] and $O[(N_x N_y)^2 N_z]$ using the nested dissection technique [20], presenting great limitations on the cross-section size of simulated devices. Currently, the NEGF+TB method with the minimal representation is capable of simulating device materials comprising more than 100,000 atoms [21], while the first-principles NEGF+DFT method, for example, with the linear combination of the atomic orbital method, can simulate materials with a few thousand atoms [11], still far from the size of a realistic nanotransistor. Moreover, the inclusion of important electron-phonon coupling and other complex interactions can significantly complicate the calculation of NEGF, seriously limiting the application of NEGF-based quantum transport simulations [15].

Therefore, the development of a new representation of NEGF with significantly reduced computational complexity is highly desirable for quantum transport simulation of large-scale device materials and for matching the demand in modern semiconductor research. In this work, we propose an approach by introducing the stochastic representation of NEGF, termed the random NEGF (rNEGF) method, to calculate the quantum transport properties of large-scale device materials. The rNEGF method significantly reduces the computational complexity of NEGF to solving a small set of linear equations, and bares only the statistical error. We demonstrate the effectiveness of the rNEGF method by combining with the first-principles quantum transport method to calculate transmission through a disordered device with large planar supercell size.

We consider a large two-probe device containing a disordered central device region sandwiched by the left and right semi-infinite electrodes as shown in Fig. 1. The size of the device is denoted by the cross section of the planar supercell size $N_x N_y$ atoms and the length size of the N_z atomic monolayers (MLs) in the transport direction including the buffer layers. To start, we introduce the rNEGF, namely the random lesser GF, for the central device as

$$\tilde{G}_{cc}^{<} = G_{cc}^{\mathcal{R}} \tilde{\Sigma}^{<} G_{cc}^{\mathcal{A}}, \quad (1)$$

where $G_{cc}^{\mathcal{R}}$ and $G_{cc}^{\mathcal{A}} = G_{cc}^{\mathcal{R}\dagger}$ are the respective retarded and advanced GFs, and $\tilde{\Sigma}^{<}$ is a random representation of lesser self-energy due to electrodes. Here, $G_{cc}^{\mathcal{R}} = (E^+ O_{cc} - H_{cc} - \Sigma_l^{\mathcal{R}} - \Sigma_r^{\mathcal{R}})^{-1}$, where O_{cc} and H_{cc} are the respective overlap and Hamiltonian matrices of the device, and $\Sigma_{l/r}^{\mathcal{R}}$ are retarded self energies of left and right electrodes. To introduce the random $\tilde{\Sigma}^{<}$, we make the eigenstate decomposition to the Hermitian linewidth function $\Gamma_{l/r} = i(\Sigma_{l/r}^{\mathcal{R}} - \Sigma_{l/r}^{\mathcal{A}})$, which characterizes the effects of coupling between the electrodes

*Contact author: keyq@shanghaitech.edu.cn

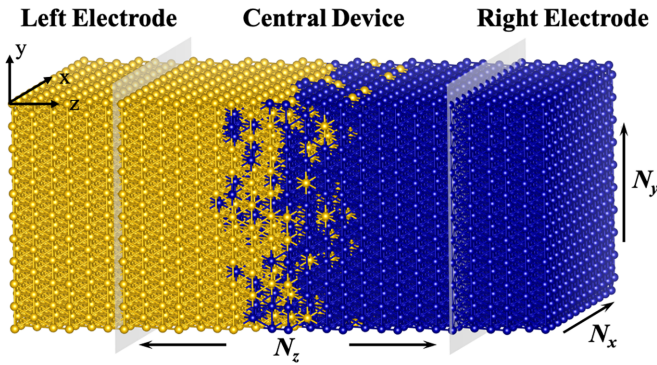


FIG. 1. Schematic illustration of two-probe device containing a central device region contacting to the left and right electrodes. The device features a large planar supercell size (denoted by $N_x \times N_y$ atoms) and N_z atomic monolayers (including the buffer layers) in transport direction.

and central device region [22]:

$$\Gamma_{l/r} = \sum_{i=1}^{N_{l/r,\text{mode}}} |\Phi_{l/r,i}\rangle v_{l/r,i} \langle \Phi_{l/r,i}| = U_{l/r} V_{l/r} U_{l/r}^\dagger. \quad (2)$$

Here, $\Phi_{l/r,i}$ are the source eigenmodes, and the eigen value $v_{l/r,i}$ presents the velocity of the eigenmode from electrodes [23]. Here, $N_{l/r,\text{mode}}$ denotes the total number of source modes (or scattering states). We neglect all the eigenmodes with velocity close to zero, and $N_{l/r,\text{mode}}$ is thus usually much smaller than the size of $\Gamma_{l/r}$. It is important to note that the source eigenmode space of N_{mode} provides a minimal and adequate representation for Γ and then for calculating NEGF. However, $N_{l/r,\text{mode}} \propto N_x N_y$ presents important challenge for large scale quantum transport simulation with the conventional method.

We then introduce the random representation of $\Gamma_{l/r}$ by

$$\tilde{\Gamma}_{l/r} = U_{l/r} \sqrt{V_{l/r}} \tilde{I}_{l/r} \sqrt{V_{l/r}} U_{l/r}^\dagger. \quad (3)$$

Here, the random resolution of identity matrices or projector $\tilde{I}_{l/r}$ are defined as

$$\tilde{I}_{l/r} = \frac{1}{N_s} \sum_{j=1}^{N_s} |X_{l/r,j}\rangle \langle X_{l/r,j}|, \quad (4)$$

where the random state $|X_{l/r,j}\rangle$ is a superposition of the source eigenmodes, and is generated by randomly choosing 1 or -1 with equal probability for each element, e.g., $|X_{l/r,j}\rangle = (1, -1, \dots, -1)^\dagger$ with a dimension of $N_{l/r,\text{mode}}$, ensuring all eigenmodes are equally sampled (other choices of random states are possible) [24]. It is clear that $\langle \tilde{I}_{l/r} \rangle = I_{l/r}$ by ensemble average, and thus the random states form a nearly complete representation space, providing the statistical correctness of rNEGF method. As a result,

$$\tilde{\Gamma}_{l/r} = \frac{1}{N_s} \sum_{j=1}^{N_s} |R_{l/r,j}\rangle \langle R_{l/r,j}|, \quad (5)$$

where $|R_{l/r,j}\rangle = U_{l/r} \sqrt{V_{l/r}} |X_{l/r,j}\rangle$. The random lesser self-energy is then defined as

$$\tilde{\Sigma}^< = i f_l \tilde{\Gamma}_l + i f_r \tilde{\Gamma}_r \quad (6)$$

with $f_{l/r}$ denoting the Fermi-Dirac distribution function in electrodes. As a result, we obtain for the lesser GF in Eq. (1)

$$\tilde{G}_{cc}^< = \frac{1}{N_s} \sum_{j=1}^{N_s} i f_l |\alpha_{l,j}\rangle \langle \alpha_{l,j}| + i f_r |\alpha_{r,j}\rangle \langle \alpha_{r,j}|, \quad (7)$$

where $|\alpha_{l/r,j}\rangle = G_{cc}^{\mathcal{R}} |R_{l/r,j}\rangle$ is called the random scattering state, and is obtained by

$$(E^\dagger O_{cc} - H_{cc} - \Sigma_l^{\mathcal{R}} - \Sigma_r^{\mathcal{R}}) |\alpha_{l/r,j}\rangle = |R_{l/r,j}\rangle. \quad (8)$$

The computation of random NEGF is thus reduced to solving N_s linear equations. To solve the linear equations above, direct solvers, including the Lower-Upper (LU), Cholesky factorization, and nested dissection method [25], and the linear-scaling iterative methods, e.g., Krylov subspace [26] and multigrid methods [27], can be applied to achieve an efficient calculation of rNEGF and related transport properties.

The rNEGF bares the statistical error, and it is expected that N_s much smaller than the number of source eigenmodes $N_{l/r,\text{mode}}$ can provide good accuracy for a large scale device (as demonstrated for the random equilibrium GF method which has shown important accuracy for equilibrium density matrix and the total energy) [24]. It is important to mention that other different random representations of NEGF exist, including $G_{cc}^< \tilde{I}_{cc}$ same as we previously proposed for random equilibrium GF in Ref. [24] and using $\Sigma_{l/r}^< \tilde{I}_{l/r}$ in Eq. (1) as we included in the Supplemental Material [44], but present much larger statistical error compared to the present method (with the same N_s). (we have tested the strategy using $G_{cc}^< \tilde{I}_{cc}$ presents larger error than that of using $\Sigma_{l/r}^< \tilde{I}_{l/r}$). In Eq. (4) for $\tilde{I}_{l/r}$, the randomness is introduced on the adequate and minimal degrees of freedom for rNEGF, namely the eigen-mode space of $\Gamma_{l/r}$, which is much smaller than space sizes of $\tilde{I}_{l/r}$ and \tilde{I}_{cc} which are the respective sizes of $\Sigma^<$ and G_{cc} . Therefore, we believe the present sampling of random states within the eigenmode space of $\Gamma_{l/r}$ in Eqs. (3) and (4) realizes the “importance sampling” for rNEGF, and thus minimizes the statistical deviation of results and N_s , compared to our previous report of random equilibrium GF method [24] and the one in Supplemental Material [44]. As an important application of rNEGF for quantum transport, here we calculate the transmission coefficient for electron transport through a two-probe device in Fig. 1, given by the formula $T(E) = \text{Tr}[G_{cc}^{\mathcal{R}} \Gamma_l G_{cc}^{\mathcal{A}} \Gamma_r]$ [22]. At zero temperature, we can set $f_l = 1$ and $f_r = 0$, the transmission coefficient can be rewritten as $T(E) = \text{Tr}[-i G_{cc}^< \Gamma_r]$ [28]. Then, with the rNEGF in Eq. (7), the transmission coefficient can be calculated as

$$\tilde{T}(E) = \frac{1}{N_s} \sum_{j=1}^{N_s} \langle \alpha_{l,j} | \Gamma_r | \alpha_{l,j} \rangle, \quad (9)$$

providing a stochastic calculation of quantum transport property for large-scale devices. As we will show, a rather small N_s , in orders of magnitude smaller than $N_{l/r,\text{mode}}$ in Eq. (2), provides accurate transmission for large device.

As the first demonstration, we implement the rNEGF method within the exact muffin-tin orbital (EMTO) based first-principles device-materials simulation package SIGMAX [29–34]. The EMTO features the high localization and minimal basis set, and thus provides an effective

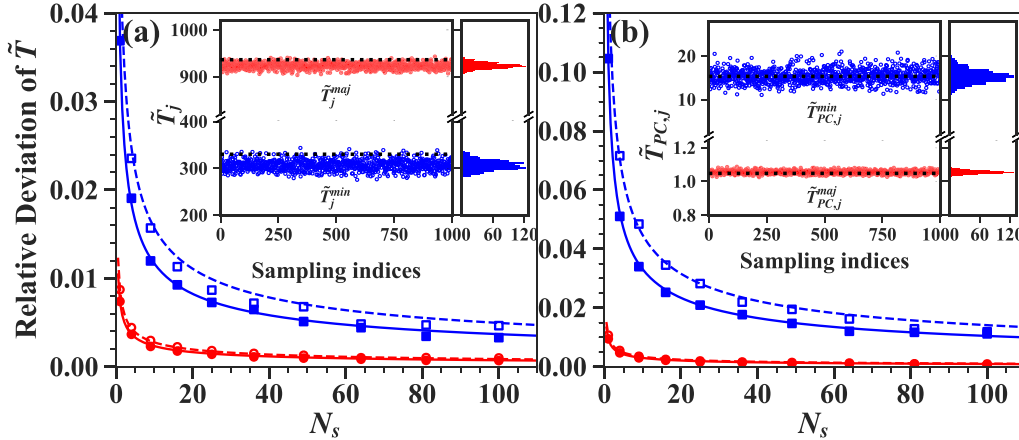


FIG. 2. Relative standard deviation of transmission versus N_s for different spin channels in systems (a) Cu/(12ML)Cu_{0.5}Co_{0.5}/Co and (b) Fe/(2ML)Fe_{0.7}Co_{0.3}/(5ML)Va/(2ML)Fe_{0.7}Co_{0.3}/Fe. The solid and hollow markers are for the respective systems with $N_x = N_y = 40$ and 30. The solid and dashed lines are fitting to the relation of $\sigma_{N_s} \propto 1/\sqrt{N_s}$. Circles and squares indicate the majority and minority spin channels, respectively. Inset: T_j versus index of random states for different spin channels for systems with planar supercell of $N_x = N_y = 40$.

implementation of Kohn-Sham DFT [35–38]. To test the capability of rNEGF-EMTO-DFT method, we calculate the transmission for two different devices in diffusive transport regime, including disordered Cu/12(ML)Cu_{0.5}Co_{0.5}/Co metallic multilayer along FCC(111) with $N_z = 24$, and disordered magnetic tunneling junction (MTJ) Fe/2(ML)Fe_{0.7}Co_{0.3}/5(ML)Va/2(ML)Fe_{0.7}Co_{0.3}/Fe along BCC(100) with $N_z = 20$ (Va denotes the vacuum atomic sphere). For both devices, the planar supercell sizes of $N_x = N_y = 30$ and 40 are used to accommodate the disorder scenarios. It should be noted that vacuum-based MTJ features dominant resonant tunneling, which is contributed by the few special resonant states in the minority spin channel (in parallel configuration) [31,33,39–41], and thus presents an important test for the validity of the rNEGF method. The spd 9 orbitals are used for each atomic sphere. For both supercell devices, all transmission results are calculated for $\vec{k}_\parallel = 0$, and all atomic potentials in spherical cell approximation [37] are obtained by EMTO-DFT in combination with coherent potential approximation with the exchange correlation potential treated by a local spin-density approximation [42,43]. Since the electrodes are perfect, the supercell self-energies $\Sigma_{l/r}^R$ and $\Gamma_{l/r}$ are then obtained by the folding technique based on primitive cell calculations, as shown in the Supplemental Material [44]. All linear equations of rNEGF are solved by nested dissection method in MUMPS [45] on a single node of Intel Xeon Gold 6226 CPU (2.70GHz) with 32 cores. For comparison, we also calculated the transmission using the nonequilibrium dynamical cluster approximation (NEDCA) for the mean-field treatment of disorder average at nonequilibrium [29,31,46].

In the insets of Fig. 2, we present $\tilde{T}_j(E_F) = \langle \alpha_{l,j} | \Gamma_r | \alpha_{l,j} \rangle$ of each random state for the majority and minority spin channels in the disordered Cu/Co multilayer in (a), and MTJ in parallel configuration (PC) in (b) with $N_x = N_y = 40$. The transmission coefficients are calculated at the Fermi level of the devices, which are -0.1075 Ry and -0.0883 Ry for the respective Cu/Co junction and MTJ. For both device systems, \tilde{T}_j^{maj} and \tilde{T}_j^{min} exhibit stochastic fluctuation around their mean

value and follow a distribution close to the Gaussian function. All mean values $\langle T \rangle$ of rNEGF are found to be in very good agreement with the NEDCA mean-field results (dotted lines in insets), for example, for the respective Cu/Co interface and MTJ in PC, $\langle T^{\text{maj}} \rangle = 923.34$ and 1.05 and $\langle T^{\text{min}} \rangle = 306.45$ and 15.5, compared to the corresponding NEDCA results 936.3, 1.05, 330.2, and 15.3, demonstrating the validity of rNEGF for the calculation of quantum transport.

In Fig. 2, we investigate the relative deviation of the transmission coefficient versus N_s , namely $\delta_{N_s} = \Delta_{N_s}/\langle T \rangle$ (Δ_{N_s} is the standard deviation of transmission with N_s random states). The small magnitude of δ_{N_s} with small N_s characterizes the effectiveness or efficiency of rNEGF for the calculation of large-scale devices. As shown, δ_{N_s} for both disordered systems exhibits small magnitude and fast decrease as N_s . Specifically, for both systems with $40 \times 40 \times 24$ atoms as shown in Figs. 2(a) and 2(b), the values of $\delta_{N_s}^{\text{maj}}$ at even $N_s = 1$ are surprisingly small, namely 0.7% for Cu/Co and 0.9% for the MTJ, providing a highly effective quantum transport calculation for these spin channels with rNEGF. Both Cu/Co and MTJ present $\delta_{N_s}^{\text{min}}$ much larger than $\delta_{N_s}^{\text{maj}}$, for example, at $N_s = 1$, $\delta_{N_s}^{\text{min}} = 3.6\%$ for Cu/Co and 10.46% for MTJ in PC. The large magnitude of $\delta_{N_s}^{\text{min}}$ reflects the large fluctuation of transmission in the eigenmode space, which requires more random states samplings to reduce the standard deviation. For example, the large magnitude of $\delta_{N_s}^{\text{min}}$ in the MTJ of PC can be attributed to the dominant resonant tunneling due to the few resonant scattering states known for the hot spots in transmission [31,33,39,47], and thus provides an important test case for the rNEGF method. It can be found that, with $N_s = 10$, $\delta_{N_s}^{\text{min}}$ for Cu/Co is rapidly decreased to 1.1%, while $\delta_{N_s,PC}^{\text{min}}$ is reduced to 2.5% with $N_s = 16$, and 1.2% with $N_s = 64$, which captures the resonant tunneling. For both systems, it is clear that, to reach the relative deviation $\delta_{N_s} \sim 1\%$, the required N_s is rather small and is orders of magnitude smaller than the corresponding number of source eigenmodes, e.g., $N_{l,\text{mode}} = 1275$ for each spin in the Cu electrode of the Cu/Co, $N_{l,\text{mode}} = 2906$ and 1618 for the respective majority and minority spins

in the Fe electrode of the MTJ (where the dimension of the matrix Γ_l is 14400). This comparison demonstrates the high effectiveness of rNEGF for the calculation of transport compared to previous recursive GF [19] and scattering state approaches [48]. It is worth emphasizing that our proposed random NEGF method incorporates an importance sampling strategy that can significantly reduce both the statistical error and the number of random states N_s . To demonstrate the advantages of this approach, we have provided transmission results without the importance sampling, namely using the rNEGF with $\tilde{\Sigma}_{l/r}^< = \Sigma_{l/r}^< \tilde{I}_{l/r}$ in Eq. (1), for comparison in the supplement (see Fig. S1) [44]. As shown in Fig. S1, at $N_s = 1$, the values of $\sigma_{N_s}^{maj(min)}$ for the disordered Cu/Co system with $40 \times 40 \times 24$ atoms and MTJ in PC with $40 \times 40 \times 20$ atoms are the respective 5.14% (7.88%) and 12.9% (42.2%), which are all significantly larger than the corresponding results of the present Fig. 2 with the importance sampling.

As shown in Fig. 2 for both systems, we find that the results of δ_{N_s} all fit very well to the relation $\delta_{N_s} = \delta_{N_s}|_{N_s=1}/\sqrt{N_s}$, consistent with the central limit theorem [49]. Furthermore, we find that, for a fixed N_s , enlarging the size of the planar supercell reduces the relative deviations δ_{N_s} , presenting an important effect of self-averaging with respect to the cross-section size. Compared to the results of the supercell $N_x = N_y = 30$ in hollow makers as shown in Fig. 2, the δ_{N_s} results of supercell $N_x = N_y = 40$ are reduced by a factor of $\frac{3}{4}$, revealing the fact that δ_{N_s} depends on the size of the system by the relation $\delta_{N_s} \propto 1/\sqrt{N_x N_y}$. It has been analytically proven that [49] for the random state method, the deviation of the averaged global quantity scales as $1/\sqrt{N_{dof}}$, where N_{dof} denotes the number of degrees of freedom in random states (which is the N_{mode} that is proportional to $N_x N_y$ in the present approach.) As a result, we conclude the relative deviation of transmission for large-scale system scales as $1/\sqrt{N_s N_x N_y}$ with the rNEGF method, presenting the important feature of random-state representation [49]. It is thus expected that, for systems with large enough $N_x N_y$, the rNEGF calculation with $N_s = 1$ can provide accurate transmission results. Compared to other cases, the rNEGF method for the resonant tunneling transport in the minority spin channel of MTJ in PC presents a relatively weaker self-averaging effect, and thus a larger standard deviation in the transmission for representation with random states.

To further test the effectiveness of the rNEGF method for the transmission calculation, we present $\tilde{T}(E)/N_x N_y$ for different energies in the range $-0.5 \leq E - E_F \leq 0.5$ eV and compare with the NEDCA results in Fig. 3. For all rNEGF calculations, we use $N_x = N_y = 30$ planar supercell. For both disordered Cu/Co multilayer and MTJ (including PC and antiparallel configuration [APC]), it is clear that the rNEGF results agree well with the NEDCA calculations in the entire energy range. In particular, for the Cu/Co system as shown in Fig. 3(a), by using only $N_s = 10$ and 1 for the respective minority and majority spin channels, the relative deviation (error bar) of rNEGF maintains at $\sim 1\%$ for all calculated energy points. For vacuum-based MTJ as shown in Fig. 3(b), $N_s = 1, 40$ and 10 for the respective majority, the minority spins in PC and APC are required to reach δ_{N_s} below 2% at all calculated energy points. It is worth noting that the values

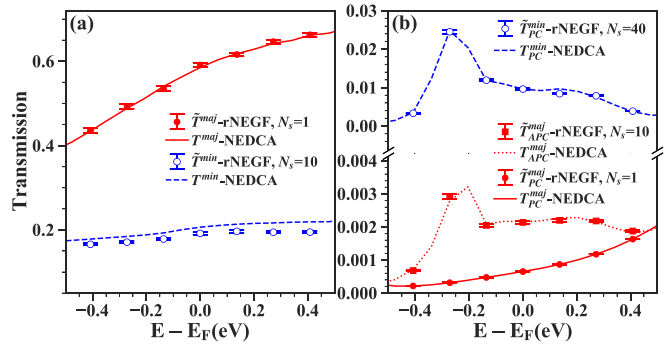


FIG. 3. Transmission versus energy for different spin channels in the systems (a) Cu/(12ML)Cu_{0.5}Co_{0.5}/Co and (b) Fe/-(2ML)Fe_{0.7}Co_{0.3}/(5ML)Va/(2ML)Fe_{0.7}Co_{0.3}/Fe. The lines are for the NEDCA results, and the markers with error bar are for the results of rNEGF calculation with planar supercell $N_x = N_y = 30$.

of T_{PC}^{\min} are approximately one order of magnitude larger than $T_{\text{PC}}^{\text{maj}}$ and $T_{\text{APC}}^{\text{maj}}$ (very close to T_{APC}^{\min}), due to the presence of resonant tunneling in the minority spin channel of the PC of the MTJ. Therefore, we see the fact that a rather small N_s can ensure a very small magnitude of $\delta_{N_s}(E)$ for a wide range of energy, demonstrating the important effectiveness of the rNEGF method for large-scale quantum transport simulation.

Concerning the computational efficiency of rNEGF method compared to the exact scattering-state method, we divide the solution of Eq. (8) into two steps, including the first step of LU decomposition and the second step of applying L and U to solve the scattering states. If we use the same method to solve for the exact scattering states and random scattering states, the computational and memory cost for the first step is the same. However, rNEGF calculation almost eliminates the computational cost of the second step, reduced by 2 to 3 orders of magnitude compared to the exact method. Taking Cu/Co junction with $40 \times 40 \times 24$ atoms as an example, the total CPU time for the first step LU decomposition is 5500 seconds per spin channel. In the second step, solving a single scattering state takes around 90 seconds on average. Thus, for an exact calculation involving $N_{\text{mode}} = 1275$ scattering states per spin channel, the second step alone requires 114750 seconds per spin channel, which is over 20 times larger than the LU decomposition, dominating the overall computational cost. The situation becomes even worse for the exact method when N_{mode} increases with increasing $N_x N_y$. In contrast, the required N_s by using rNEGF method can decrease with increasing $N_x N_y$ due to the self-average effect of the approach. As the LU decomposition dominates the computational expense of the rNEGF method, a faster and more memory-efficient LU decomposition algorithm is essential for its application to larger systems. Such an algorithm exists [50], and we are working on it to further enhance the performance of rNEGF method.

In summary, we have developed the rNEGF for large-scale quantum transport simulation. The rNEGF is represented by N_s random superposition states of source eigenmodes, and its computation is reduced to solving N_s linear equations. The rNEGF method only bears the statistical error. As a first demonstration, we have implemented rNEGF with the

EMTO-based DFT method and applied it to calculate the transmission coefficient for the large disordered structures. It is found that a rather small N_s (even $N_s = 1$), in orders of magnitude smaller than the eigenmodes, can produce a reliable transport property with the relative standard deviation $\sim 1\%$. The rNEGF quantum transport method possesses an important self-averaging effect with respect to the cross-section size of the device, presenting an effective stochastic quantum transport approach. The rNEGF method can be generally utilized for large-scale tight-binding device models and

phonon quantum transport, and is potentially applicable to large-scale nonequilibrium quantum many-body problems.

Y.K. acknowledges financial support from NSFC (Grant No. 12227901). L.W. and K.X. acknowledge financial support from the National Key Research and Development Program of China (Grants No. 2023YFA1406600 and No. 2021YFA1202200). The authors thank the HPC platform of ShanghaiTech University for providing the computational facility.

-
- [1] J. Schwinger, Brownian motion of a quantum oscillator, *J. Math. Phys.* **2**, 407 (1961).
 - [2] L. Kadanoff and G. Baym, *Quantum Statistical Mechanics: Green's Function Methods in Equilibrium and Nonequilibrium Problems*, Frontiers in Physics. A Lecture Note and Reprint Series (W.A. Benjamin, London, 1962)
 - [3] L. V. Keldysh, Diagram technique for nonequilibrium processes, *Sov. Phys.-JETP* **20**, 1018 (1965).
 - [4] K.-C. Chou, Z.-B. Su, B.-L. Hao, and L. Yu, Equilibrium and nonequilibrium formalisms made unified, *Phys. Rep.* **118**, 1 (1985).
 - [5] H. Haug and A. Jauho, *Quantum Kinetics in Transport and Optics of Semiconductors*, Springer Series in Solid-State Sciences (Springer, Berlin, 2007).
 - [6] G. Stefanucci and R. van Leeuwen, *Nonequilibrium Many-Body Theory of Quantum Systems: A Modern Introduction* (Cambridge University Press, Cambridge, 2013).
 - [7] S. Steiger, M. Povolotskyi, H.-H. Park, T. Kubis, and G. Klimeck, Nemo5: A parallel multiscale nanoelectronics modeling tool, *IEEE Trans. Nanotechnol.* **10**, 1464 (2011).
 - [8] J. Taylor, H. Guo, and J. Wang, *Ab initio* modeling of quantum transport properties of molecular electronic devices, *Phys. Rev. B* **63**, 245407 (2001).
 - [9] M. Brandbyge, J.-L. Mozos, P. Ordejón, J. Taylor, and K. Stokbro, Density-functional method for nonequilibrium electron transport, *Phys. Rev. B* **65**, 165401 (2002).
 - [10] Y. Ke, K. Xia, and H. Guo, Disorder scattering in magnetic tunnel junctions: Theory of nonequilibrium vertex correction, *Phys. Rev. Lett.* **100**, 166805 (2008).
 - [11] <https://www.synopsys.com/manufacturing/quantumatk.html>.
 - [12] <https://nanoacademic.com/solutions/nanodcal>.
 - [13] N. Papior, N. Lorente, T. Frederiksen, A. García, and M. Brandbyge, Improvements on non-equilibrium and transport green function techniques: The next-generation transiesta, *Comput. Phys. Commun.* **212**, 8 (2017).
 - [14] R. A. Bell, S. M.-M. Dubois, M. C. Payne, and A. A. Mostofi, Electronic transport calculations in the onetep code: Implementation and applications, *Comput. Phys. Commun.* **193**, 78 (2015).
 - [15] A. N. Ziogas, T. Ben-Nun, G. I. Fernández, T. Schneider, M. Luisier, and T. Hoefer, A data-centric approach to extreme-scale *ab initio* dissipative quantum transport simulations, in *Proceedings of the International Conference for High Performance Computing, Networking, Storage and Analysis, SC '19* (Association for Computing Machinery, New York, 2019), pp. 1–13.
 - [16] M. Luisier, A. Schenk, W. Fichtner, and G. Klimeck, Atomistic simulation of nanowires in the $sp^3d^5s^*$ tight-binding formalism: From boundary conditions to strain calculations, *Phys. Rev. B* **74**, 205323 (2006).
 - [17] J. Ferrer, C. J. Lambert, V. M. García-Suárez, D. Z. Manrique, D. Visontai, L. Oroszlany, R. Rodríguez-Ferradás, I. Grace, S. W. D. Bailey, K. Gillemot, H. Sadeghi, and L. A. Algharagholy, Gollum: A next-generation simulation tool for electron, thermal and spin transport, *New J. Phys.* **16**, 093029 (2014).
 - [18] D. Marian, E. Marin, M. Perucchini, G. Iannaccone, and G. Fiori, Multi-scale simulations of two dimensional material based devices: The nanotcad vides suite, *J. Comput. Electron.* **22**, 1327 (2023).
 - [19] E. M. Godfrin, A method to compute the inverse of an n-block tridiagonal quasi-Hermitian matrix, *J. Phys.: Condens. Matter* **3**, 7843 (1991).
 - [20] U. Hetmaniuk, Y. Zhao, and M. Anantram, A nested dissection approach to modeling transport in nanodevices: Algorithms and applications, *Int. J. Numer. Meth. Eng.* **95**, 587 (2013).
 - [21] <https://engineering.purdue.edu/gekcogrp/software-projects/nemo5>.
 - [22] S. Datta, *Quantum Transport: Atom to Transistor* (Cambridge University Press, Cambridge, 2005).
 - [23] P. A. Khomyakov, G. Brocks, V. Karpan, M. Zwierzycki, and P. J. Kelly, Conductance calculations for quantum wires and interfaces: Mode matching and Green's functions, *Phys. Rev. B* **72**, 035450 (2005).
 - [24] M. Tang, C. Liu, A. Zhang, Q. Zhang, J. Zhai, S. Yuan, and Y. Ke, Random Green's function method for large-scale electronic structure calculation, *Chin. Phys. Lett.* **41**, 053102 (2024), Express Lett..
 - [25] A. George, Nested dissection of a regular finite element mesh, *SIAM J. Numer. Anal.* **10**, 345 (1973).
 - [26] T. Hoshi, S. Yamamoto, T. Fujiwara, T. Sogabe, and S.-L. Zhang, An order-n electronic structure theory with generalized eigenvalue equations and its application to a ten-million-atom system, *J. Phys.: Condens. Matter* **24**, 165502 (2012).
 - [27] R. Wienands and W. Joppich, *Practical Fourier Analysis for Multigrid Methods*, Numerical Insights (Taylor & Francis, London, 2005).
 - [28] J. Yan and Y. Ke, Generalized nonequilibrium vertex correction method in coherent medium theory for quantum transport simulation of disordered nanoelectronics, *Phys. Rev. B* **94**, 045424 (2016).

- [29] Q. Zhang, J. Yan, Y. Zhang, and Y. Ke, Exact muffin tin orbital based first-principles method for electronic-structure and electron-transport simulation of device materials, *Phys. Rev. B* **100**, 075134 (2019).
- [30] Z. Chen, Q. Zhang, Y. Zhang, L. Wang, M. Sang, and Y. Ke, Exact muffin-tin orbital based fully relativistic simulation of device materials: Electronic charge and spin current, *Phys. Rev. B* **102**, 035405 (2020).
- [31] Y. Zhang, J. Zhai, Z. Chen, Q. Zhang, and Y. Ke, First-principles nonequilibrium dynamical cluster theory for quantum transport simulations of disordered nanoelectronic devices, *Phys. Rev. B* **104**, 115412 (2021).
- [32] Z. Chen, Q. Zhang, Z. Yuan, J. Liu, K. Xia, and Y. Ke, Fully relativistic first-principles quantum transport simulation of non-collinear spin transfer and spin hall current, *Phys. Rev. B* **107**, 195431 (2023).
- [33] Y. Zhang, Q. Zhang, Y. Ke, and K. Xia, Giant influence of clustering and anti-clustering of disordered surface roughness on electronic tunneling, *Chin. Phys. Lett.* **39**, 087301 (2022).
- [34] C. Hu, Y. Zhang, Z. Chen, Q. Zhang, J. Zhu, S. Hu, and Y. Ke, Size effect of resistivity due to surface roughness scattering in alternative interconnect metals: Cu, Co, Ru, and Mo, *Phys. Rev. B* **107**, 195422 (2023).
- [35] O. K. Andersen, C. Arcangeli, R. W. Tank, T. Saha-Dasgupta, G. Krier, O. Jepsen, and I. Dasgupta, Third-generation tb-lmto, *MRS Proceedings* **491**, 3 (1997).
- [36] O. K. Andersen and T. Saha-Dasgupta, Muffin-tin orbitals of arbitrary order, *Phys. Rev. B* **62**, R16219 (2000).
- [37] L. Vitos, H. Skriver, B. Johansson, and J. Kollár, Application of the exact muffin-tin orbitals theory: the spherical cell approximation, *Comput. Mater. Sci.* **18**, 24 (2000).
- [38] L. Vitos, *Computational Quantum Mechanics for Materials Engineers: The EMTO Method and Applications* (Springer London, London, 2007).
- [39] P. X. Xu, V. M. Karpan, K. Xia, M. Zwierzycki, I. Marushchenko, and P. J. Kelly, Influence of roughness and disorder on tunneling magnetoresistance, *Phys. Rev. B* **73**, 180402(R) (2006).
- [40] K. Liu, K. Xia, and G. E. W. Bauer, Shot noise in magnetic tunnel junctions from first principles, *Phys. Rev. B* **86**, 020408(R) (2012).
- [41] J. Yan, S. Wang, K. Xia, and Y. Ke, Anomalous spin-dependent tunneling statistics in fe/mgo/fe junctions induced by disorder at the interface, *Phys. Rev. B* **97**, 014404 (2018).
- [42] D. M. Ceperley and B. J. Alder, Ground state of the electron gas by a stochastic method, *Phys. Rev. Lett.* **45**, 566 (1980).
- [43] J. P. Perdew and A. Zunger, Self-interaction correction to density-functional approximations for many-electron systems, *Phys. Rev. B* **23**, 5048 (1981).
- [44] See Supplemental Material at <http://link.aps.org/supplemental/10.1103/PhysRevB.110.155430> for (I) the calculation of supercell self-energies and Γ by folding technique based on the primitive cell calculations; (II) the transmission results without importance sampling.
- [45] <https://mumps-solver.org>.
- [46] J. Yan, S. Wang, K. Xia, and Y. Ke, First-principles quantum transport method for disordered nanoelectronics: Disorder-averaged transmission, shot noise, and device-to-device variability, *Phys. Rev. B* **95**, 125428 (2017).
- [47] W. H. Butler, X.-G. Zhang, T. C. Schultheiss, and J. M. MacLaren, Spin-dependent tunneling conductance of Fe|MgO|Fe sandwiches, *Phys. Rev. B* **63**, 054416 (2001).
- [48] K. Xia, P. J. Kelly, G. E. W. Bauer, I. Turek, J. Kudrnovský, and V. Drchal, Interface resistance of disordered magnetic multilayers, *Phys. Rev. B* **63**, 064407 (2001).
- [49] A. Hams and H. De Raedt, Fast algorithm for finding the eigenvalue distribution of very large matrices, *Phys. Rev. E* **62**, 4365 (2000).
- [50] P. Valero-Lara, C. Greenwalt, and J. S. Vetter, Sparselu, a novel algorithm and math library for sparse lu factorization, in 2022 IEEE/ACM Workshop on Irregular Applications: Architectures and Algorithms (IA3) (IEEE, Dallas, 2022), pp. 25–31.